# A High Frequency-Link Secondary-Side Phase-Shifted Full-Range Soft-Switching PWM DC-DC Converter With ZCS Active Rectifier for EV Battery Chargers

Mishima, Tomokazu

Akamatsu, Kouhei

Nakaoka, Mutsuo

(Citation)
IEEE Transactions on Power Electronics,28(12):5758-5773

(Issue Date)
2013-12

(Resource Type)
journal article

(Version)
Accepted Manuscript

# A High Frequency-Link Secondary-Side Phase-Shifted Full-Range Soft-Switching PWM DC–DC Converter with ZCS Active Rectifier for EV Battery Chargers

Tomokazu Mishima, *Member, IEEE,* Kouhei Akamatsu, *Student Member, IEEE*, and Mutsuo Nakaoka, *Member, IEEE*

***Abstract*—A new prototype of a secondary-side phase shift (SPS) soft-switching PWM dc-dc converter suitable for electric vehicle (EV) battery charging systems is presented in this paper. Wide range soft-switching operations are achievable from full load to no load by effectively utilizing the parasitic inductances of the high frequency (HF) transformer in the proposed dc-dc converter. In addition, no circulating current in both of the primary and secondary side full-bridge circuits, thereby the related idling power can be minimized. As a result, high efficiency power conversion can be maintained owing to the full range soft-switching operation and wide range output power and voltage regulations. Its operating principle is presented on the basis of theoretical analysis and simulation results, and the design procedure of the circuit parameters of the proposed dc-dc converter is described. The essential performance and its effectiveness of the proposed dc-dc converter are originally demonstrated from a practical point of view in an experiment using a $1\,\mathrm{kW}$-$50\,\mathrm{kHz}$ laboratory prototype.**

***Index Terms*—DC-DC converter, phase shift pulse width modulation (PS-PWM), soft switching, zero voltage soft switching (ZVS), zero current soft switching (ZCS), ZCS active rectifier, non-circulating current, EV battery charger.**

## I. Introduction

THE switch-mode HF-link (HF-isolated) dc-dc power converters serve as an essential power interface connecting the grid with the onboard electric power supply in a battery charging system for EVs including Plug-in HEVs (PHEVs) as introduced in Fig. 1 [1]. In particular, voltage-source full-bridge soft-switching PS-PWM dc-dc converters are suitable for the battery chargers due to the high power, low electromagnetic interference (EMI) noise emissions and applicability of versatile output power regulation schemes. The phase shift power regulation strategy is useful for the HF-link dc-dc power converter with a galvanic isolation due to precise generations of the switching signal patterns for the semiconductor power devices.

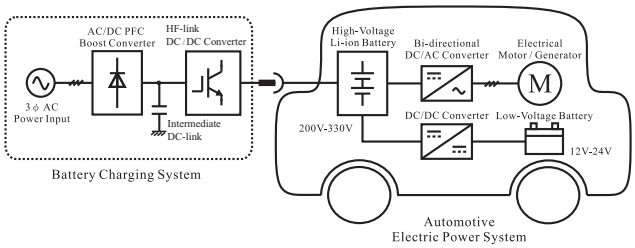


Fig. 1. Battery charging system architecture for EVs / PHEVs.

In the grid-connected battery charging system, the HF-link dc-dc converter has a function of controlling the battery voltage in a wide range with respect to the intermediate dc-link voltage which is regulated by the ac-dc rectifier. In addition, high efficiency and high reliability are essentially required in the HF-link dc-dc converter in order to enhance the total performances of the battery charging system.

As compared to the non-isolated dc-dc converter-based system in Fig. 2 (a), the HF-link dc-dc converter-applied battery charger operates with a higher switching frequency in conductive and contact-less dc-dc power conversion stages as illustrated in Fig. 2 (b) and (c). Hence, the HF-link dc-dc converter is more advantageous in term of the compact size and light weight of transformer as well as wide-range output power and voltage regulations due to a higher resolution in a controller processing.

The typical soft-switching PS-PWM dc-dc converters are based on the primary-side phase shift (PPS) scheme as depicted in Fig. 3, which have been developed not only to the automotive electric power systems but the variety of the industrial power conversion equipments. In contrast to the simplicity on the main circuit and controller, occurrence of large circulating currents and its relevant power losses are the technical issues inherent to the conventional PPS-PWM dc-dc converters in Fig. 4 [2]–[13]. In addition, ZVS ranges of the active switches especially for the active switches of the lagging phase legs in the primary-side inverter are severely limited. Besides that, the rectifier diodes in the secondary-side circuit suffer from reverse recovery currents, so that the



Manuscript received November 10, 2012; revised February 16, 2013; accepted 29 March, 2013.

T. Mishima and K. Akamatsu are with the Mechatronics Engineering Division, Graduate School of Maritime Science, Kobe University, Hyogo, Japan (e-mail: mishima@maritime.kobe-u.ac.jp).

M. Nakaoka is with The Electric Energy Saving Research Center, Kyungnam University, Republic of Korea, and Electrical & Telecommunication Engineering Division, University of Malaya, Kuala Lumper, and a professor emeritus of the Graduate School of Science & Engineering, Yamaguchi University, Yamaguchi, Japan.

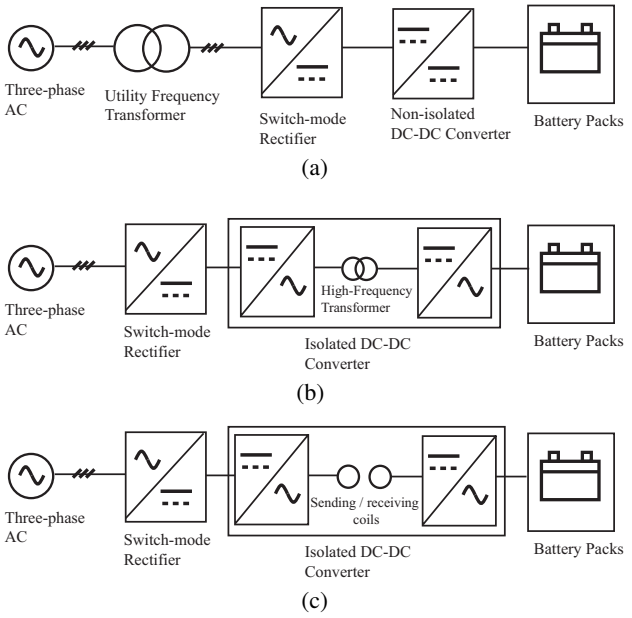


Fig. 2. Power conversion flow based on : (a) non-isolated dc-dc converter, (b) conductive HF ac-link dc-dc converter, (c) contact-less HF ac-link dc-dc converter.

power consuming RCD passive snubbers are necessary for protecting them from the voltage surges and the parasitic ringings. As a result, the conversion efficiency decreases and the higher switching frequency operations which are essential for achieving the high power density can not be performed in reality.

In order to overcome the disadvantages of the conventional ZVS PPS-PWM dc-dc converters, a variety of soft-switching PPS-PWM dc-dc converters have been developed in the past decades as summarized in Fig. 5. The improved soft-switching PPS-PWM dc-dc converters are classified into: capacitor and diodes-assisted regenerative snubbers [14], [15], switched capacitor active clamped circuit [16], [17], mode changeable active clamped circuit [18], primary-side saturable reactors [19], primary-side voltage-blocking capacitor [20], tapped-inductor filter [21], and primary-side additional resonant pole-assisted circuit [22]. Although the circulating current can be eliminated to some extent and the soft-switching limitations of the lagging phase leg can be mitigated, additional power devices and passive components are indispensable in the improved soft-switching PPS-PWM dc-dc converters. The additional magnetic components as well as capacitors cause power losses especially in the light load conditions, and are obstacles for achieving high efficiency and high power density whereas increasing a cost in developing those dc-dc converters. Furthermore, the soft-switching operations can not be ensured over the wide range of load conditions, i.e., from no load to full load.

As a counterpart PS-PWM circuit, the soft-switching SPS-PWM dc-dc converters have been developed and reported in [23]–[26]. Among them, the ZVS SPS-PWM dc-dc converter with ZVS active rectifier as depicted in Fig. 6 (a), which is more suitable for high output voltage applications, can reduce the circulating current of the primary-side inverter, but that of the secondary-side rectifier still remains [23], [24]. The ZVS SPS-PWM dc-dc converter with saturable reactor-assisted ZCS rectifier in Fig. 6 (b) has been developed by the authors [25]. In this unique dc-dc converter, the circulating currents can be eliminated in both of the primary and secondary-side power circuits. However, the additional magnetic switches are required to control the B-H curves of the saturable reactors with high sensitivity, thereby the circuit and system configuration might be complicated.

In order to overcome the drawback of the saturable reactor-assisted type, the ZVS SPS-PWM dc-dc converter with ZCS active rectifier deriving from the circuit topology of Fig. 6 (b) has been proposed by the authors in [26]. The proposed soft-switching dc-dc converter can eliminate the circulating current completely, thereby the relevant conduction power losses can be minimized without any additional passive component. Moreover, the primary-side and secondary-side active switches can operate in ZVS and ZCS for the entire load range, respectively. The soft-switching ranges on both the primary-side inverter and the secondary-side rectifier in the proposed soft-switching dc-dc converter can be extended owing to the unique current commutation process attained by the SPS-PWM scheme.

It is a remarkable feature of the proposed soft-switching SPS-PWM dc-dc converter that full-range soft-switching operations can be realized by employing the reverse conduction blocking active switches for the controlled-side leg of the rectifier. Thus, no auxiliary switch and magnetic component is required, thereby a power density of the HF-link dc-dc converter could be improved. Furthermore, the wide-range output power and output voltage regulations can be realized by a relatively small-range variation of phase shift angle. As a result, high efficiency power conversion can be expected as well as performance improvement of the battery voltage controller, which is preferable for an EV battery charging system. Although the basic and conceptual research has been reported in [26], application-specific performance evaluations on the proposed soft-switching SPS-PWM dc-dc converter including the analysis on soft-switching range and the steady-state power regulation characteristics have not been evaluated in-depth in the past relevant work.

The main objective of this paper is to originally demonstrate the operation principle, more detailed analysis on the soft-switching operations and circuit design guideline of the proposed soft-switching SPS-PWM dc-dc converter, and prove its practical effectiveness in an experiment with considerations specifically for EV battery charger applications [27]–[29]. In addition, the performances of the proposed soft-switching SPS-PWM dc-dc converter for battery charging operations is evaluated by modeling a typical constant current and constant voltage (CCCV) mode in the experiment. Furthermore, an power loss analysis is carried out for evaluating the unique circuit topology and providing more practical ideas to construct the proposed soft-switching SPS-PWM dc-dc converter.

This paper is organized as follows. The circuit configuration and operation principle together with the soft-switching conditions are explained in Section II. The soft-switching

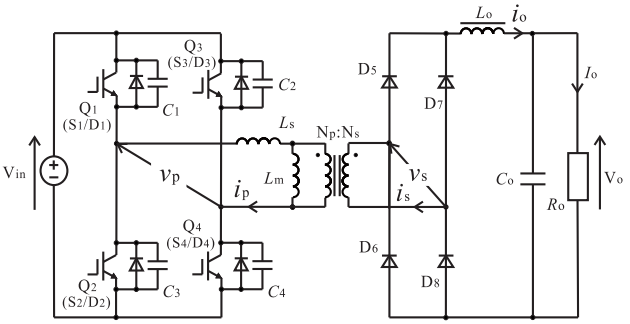


Fig. 3. A conventional ZVS PPS-PWM dc-dc converter.

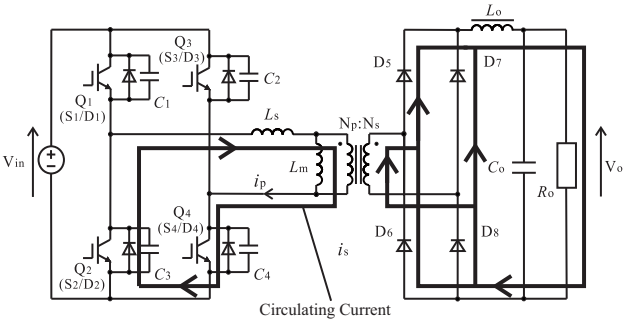


Fig. 4. A circulating current pathway in the conventional ZVS PPS-PWM dc-dc converter.

ranges, i.e. ZVS in the primary-side HF inverter and ZCS in the secondary-side active rectifier are theoretically analyzed in Section III, where the circuit design procedure is also described. In addition, the output power and output voltage vs. phase shift angle characteristics are demonstrated by theoretical analysis and its simulation results in Section IV. The performances on the output power and output voltage regulations as well as the full-range soft switching operations are actually verified by experimental results based on the prototype are provided in Section V, and effectiveness of the soft-switching SPS-PWM dc-dc converter proposed herein is evaluated from a practical point of view.

## II. Circuit Description and Operation Principle

### A. Circuit Configuration

The circuit configuration of the proposed soft-switching SPS-PWM dc-dc converter is depicted in Fig. 7. In the primary-side full bridge inverter, the lossless snubbing capacitors $C_1$–$C_4$ operate with the series inductor $L_s$ including the leakage inductance $L_k$, then ZVS turn-off and ZVS & ZCS (ZVZCS) turn-on operations can be attained all in $Q_1$–$Q_4$.

The secondary-side rectifier consists of the hybrid legs of the reverse blocking active switches $Q_5$ & $Q_6$ and diodes $D_7$ & $D_8$. The output power and output voltage can be regulated by changing the phase shift angle $\phi$ (phase shift interval $t_\phi = (\phi/360)\cdot T$) between $Q_5$ and $Q_6$ as synchronous switches with respect to $Q_1$–$Q_4$.

The features and outstanding advantages of the proposed soft-switching dc-dc converter are summarized below:

- The output power and output voltage are regulated by the active switch-mode rectifier operating at ZCS.

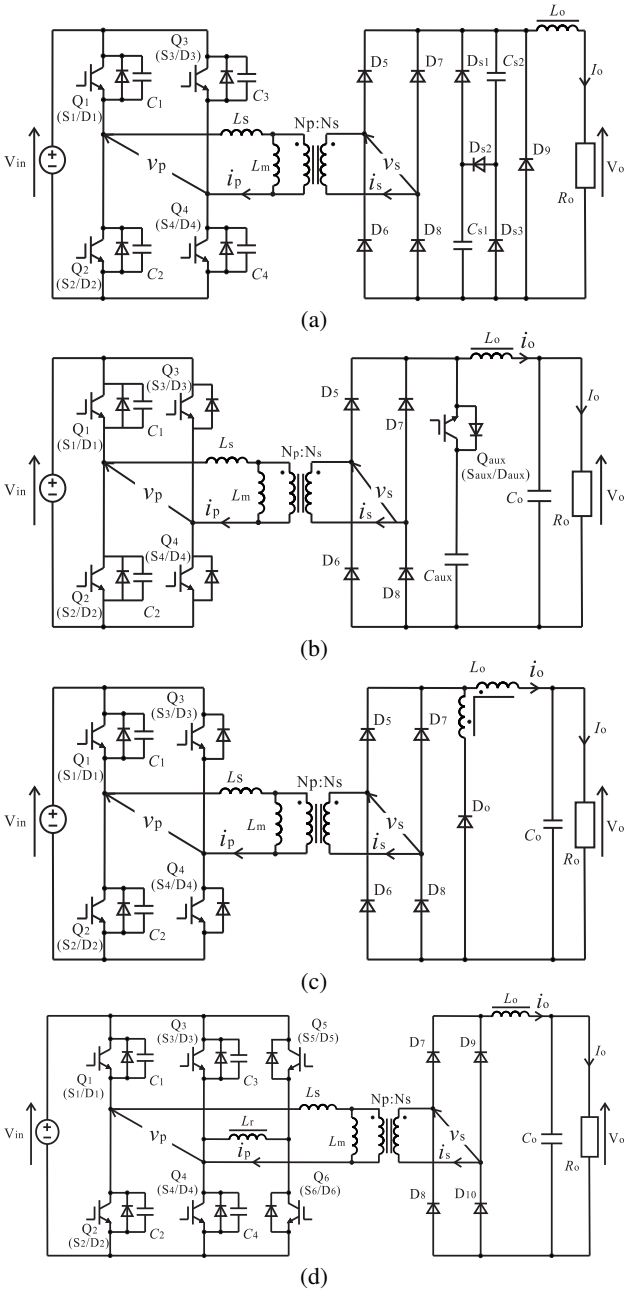


Fig. 5. Improved soft-switching PPS-PWM dc-dc converters: (a) capacitor & diode regenerative type [14], [15], (b) switched capacitor active clamp type [16], [17], (c) tapped inductor filter-assisted type [21], (d) primary-side additional resonant pole-assisted type [22].

- No additional magnetic component and capacitor is necessary as compared to the improved soft-switching PPS-PWM dc-dc converters mentioned above. This is advantageous for achieving high power density together with a light and compact size while decreasing a cost of development.
- No circulating current and the relevant power loss occurs in both of the primary and secondary-side power stages over the wide load range.
- Full-range soft-switching operations can be achieved in all of the switching power devices.
- A wide-range power regulation can be attained with the small phase shift angle variations.

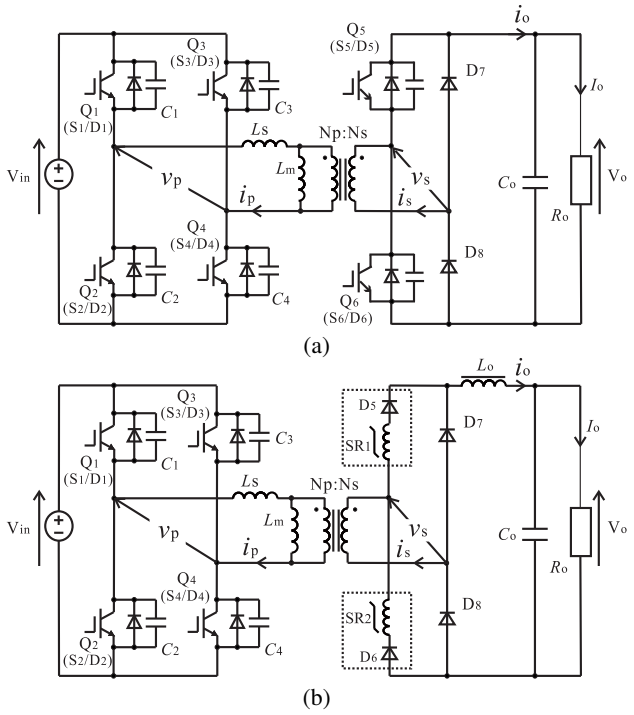


Fig. 6. Soft-switching SPS-PWM dc-dc converters: (a) ZVS active rectifier-assisted type [23], [24], (b) saturable reactor-assisted ZCS rectifier type [25].

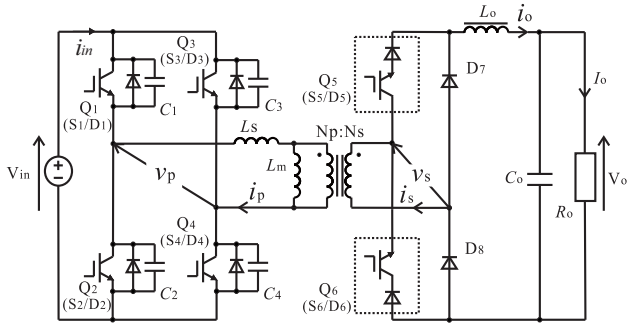

Fig. 7. Proposed soft-switching SPS-PWM dc-dc converter with ZCS active rectifier.

- The output power can be regulated linearly with the phase shift angle, thereby the control system is simpler than that of the conventional ZVS PS-PWM dc-dc converters.
- The ZCS active rectifier-assisted SPS-PWM scheme can be widely applied for other converter topologies such as half-bridge and center-tapped rectifier.

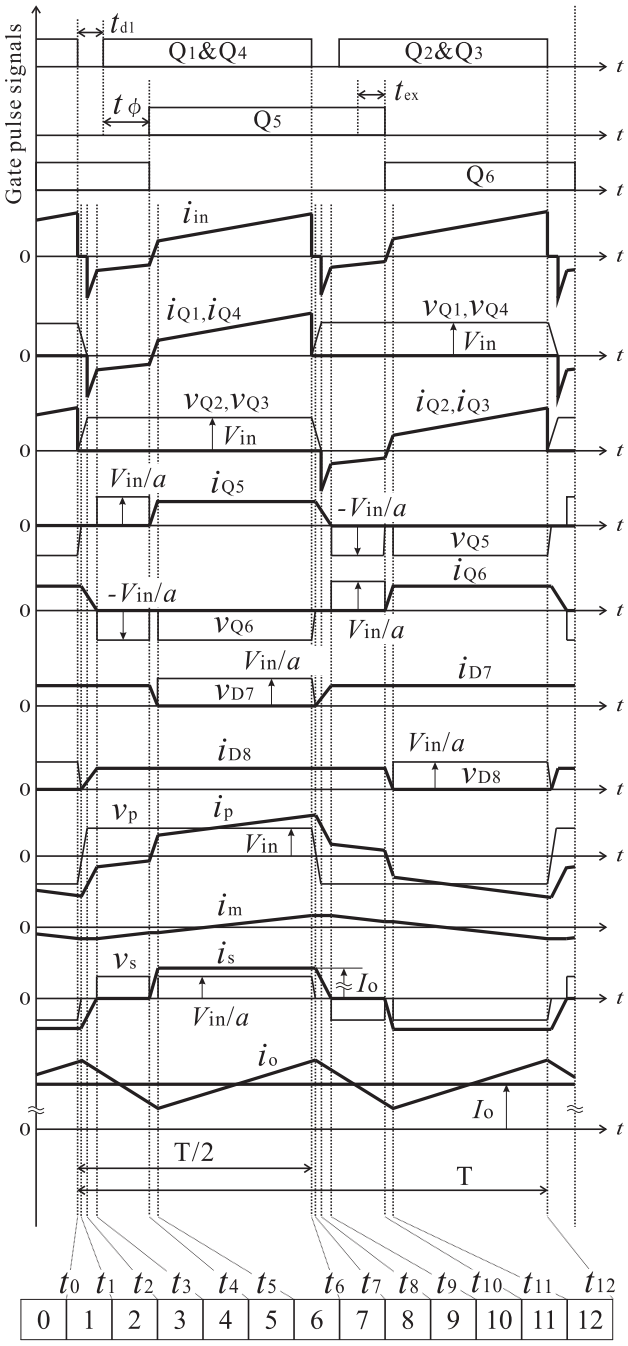


Fig. 8. Typical voltage and current operating waveforms of proposed soft-switching SPS-PWM dc-dc converter ($t_\phi = (\phi/360) \cdot T$).

### B. Operation Principle

The relevant operating waveforms are depicted in Fig. 8. The operation mode of the proposed soft-switching dc-dc converter treated herein is divided into the twelve sub-modes. The positive and negative half-cycle transitions are symmetrical, therefore only the positive half-cycle operation is explained as follows. Note here that the output smoothing inductor $L_o$ is large enough to establish $\overline{i_o(t)} = I_o$ in the secondary-side circuit.

- Mode 0 [$t < t_0$],<*steady-state power transfer mode*> The primary-side active switches $Q_2$ and $Q_3$ are on-state, while the active switch $Q_6$ and the diode $D_7$ in the secondary-side rectifier are on-state. During this mode, the electric power from the input voltage source $V_{in}$ is delivered to the load $R_o$.
- Mode 1 [$t_0 \le t < t_1$],<$Q_2$ & $Q_3$ *ZVS turn-off mode*> From the steady-state negative half-cycle in the periodical circuit operation, the gate signals for $S_2$ and $S_3$ are removed simultaneously at $t = t_0$. Then, the lossless snubbing capacitors $C_2$ and $C_3$ are charged by the inverter current $i_p$, accordingly the voltages $v_{Q2}$ and $v_{Q3}$ across $Q_2$ and $Q_3$ rise gradually due to charging of $C_2$ and $C_3$. At the same time, the voltages $v_{Q1}$ and $v_{Q4}$ across $Q_1$ and $Q_4$ decrease gradually from $V_{in}$ to zero

by discharging of $C_1$ and $C_4$. In this interval, the voltages across the primary-side active switches are expressed by defining $C_r = C_1 = C_2 = C_3 = C_4$ as

$$v_{\mathrm{Q2,Q3}}(t) = \frac{i_{mp} + I_o/a}{2C_r}(t - t_0), \quad (1)$$

$$v_{\mathrm{Q1,Q4}}(t) = V_{in} - v_{\mathrm{Q2,Q3}}(t), \quad (2)$$

where $i_{mp}$ is the peak of magnetizing current $i_m$ and $a$ denotes the winding turns ratio $N_p/N_s$ of the HF transformer.

During this interval, the primary-side inverter current $i_p(t)$ begins to decline from the negative peak current $i_p(t_0)$ as expressed by

$$i_p(t) = \frac{V_{in}}{L_s}(t - t_0) + i_p(t_0). \quad (3)$$

The soft-switching conditions in the primary-side active switches are expressed as

$$\frac{1}{2}L_s\{i_p(t_0)\}^2 \geq 2C_r{V_{in}}^2. \quad (4)$$

- Mode 2 $[t_1 \leq t < t_2]$,<$\mathrm{D_8}$ *ZCS turn-on mode*>
When the winding voltage across primary-side transformer decays to zero due to the charging and discharging of $C_1$−$C_4$ at $t = t_1$, the voltage across the secondary-side HF transformer winding terminals also becomes zero. Then, the diode $\mathrm{D_8}$ is naturally forward-biased and its current linearly rises as

$$i_{\mathrm{D8}}(t) = \frac{V_{in}}{aL_s}(t - t_1). \quad (5)$$

Thereby, ZCS turn-on can be attained in $\mathrm{D_8}$. At the same instant, the current $i_s(t)$ of HF transformer secondary-side windings declines from $i_o$ with the same gradient of (5) as

$$i_s(t) = \frac{V_{in}}{aL_s}(t - t_1) + i_o(t_1). \quad (6)$$

- Mode 3 $[t_2 \leq t < t_3]$,<*Primary-side inverter current regenerative mode*>
ZVS turn-off operations of $\mathrm{Q_2}$ and $\mathrm{Q_3}$ sustaining from Mode 1 are completed at $t = t_2$ when the voltages $v_{\mathrm{Q2}}$ and $v_{\mathrm{Q3}}$ across $\mathrm{Q_2}$ and $\mathrm{Q_3}$ reach the dc input voltage $V_{in}$. Accordingly, the voltages $v_{\mathrm{Q1}}$ and $v_{\mathrm{Q4}}$ across $\mathrm{Q_1}$ and $\mathrm{Q_4}$ are forced to be zero at $t = t_2$, then their anti-parallel diodes $\mathrm{D_1}$ and $\mathrm{D_4}$ are forward biased. During this interval, $i_p$ in the primary-side inverter keeps decreasing and approaching to zero as written by

$$i_p(t) = \frac{V_{in}}{L_s}(t - t_2) + i_p(t_2), \quad (7)$$

- Mode 4 $[t_3 \leq t < t_4]$,<$\mathrm{Q_1}$ *&* $\mathrm{Q_4}$ *ZVZCS turn-on /* $\mathrm{Q_6}$ *ZCS turn-off mode*>
When $i_p$ is equal to $i_{mp}$ at $t = t_3$, the current through the HF transformer secondary-side winding and $\mathrm{Q_6}$ decays to zero. Then, the primary-side and secondary-side power circuits are separated. In this interval, the inverter current $i_p$ of the proposed dc-dc converter is defined as

$$i_p(t) = \frac{V_{in} - aV_o}{L_s}(t - t_3) + i_p(t_3). \quad (8)$$

The inverter current $i_p$ equals to $i_m$ in this interval, and the magnetic energy of HF transformer is reset to $V_{in}$. The peak inverter current $i_p(t_0)$ is larger than or equal to $i_{mp}$ under the light load condition because $i_m$ is independent of the load current $I_o$. Therefore, the proposed dc-dc converter can achieve the soft-switching operations over the wide load range by designing $i_{mp}$. The signals for $\mathrm{S_1}$ and $\mathrm{S_4}$ are triggered while $\mathrm{D_1}$ and $\mathrm{D_4}$ are still conducting, consequently ZVZCS turn-on can be achieved in $\mathrm{Q_1}$ and $\mathrm{Q_4}$.

The current of the secondary-side active switch $i_{\mathrm{Q6}}$ decays to zero together with $i_s$. After that, the gate signal for $\mathrm{S_6}$ is removed, and the ZCS turn-off commutation can be achieved in $\mathrm{Q_6}$. In order to achieve the ZCS turn-off commutation, the turn-off timing in $\mathrm{Q_6}$ is required to be delayed by $t_{ex}$ against the turn-off timing of $\mathrm{Q_1}$, $\mathrm{Q_4}$. Using (6), $t_{ex}$ is expressed by

$$t_{ex} \geq \frac{aL_s}{V_{in}}I_o. \quad (9)$$

- Mode 5 $[t_4 \leq t < t_5]$,<$\mathrm{Q_5}$ *ZCS turn-on/ZCS turn-off mode*>
The gate of $\mathrm{S_5}$ is supplied at $t = t_4$, then $i_s$ as well as $i_p$ increases gradually due to the effect of $L_s$. Thus, the ZCS turn-on commutation can be performed in $\mathrm{Q_5}$. During this interval, $i_p$ and $i_s$ can be defined respectively as

$$i_p(t) = \frac{V_{in}}{L_s}(t - t_4) + i_p(t_4), \quad (10)$$

$$i_s(t) = a(i_p - i_m). \quad (11)$$

The HF transformer secondary-side current $i_s$ gradually commutates to $\mathrm{Q_5}$, thereby the current $i_{D7}$ through $\mathrm{D_7}$ begins to decline.

- Mode 6 $[t_5 \leq t < t_6]$,<$\mathrm{D_7}$ *positive half-cycle steady-state power transfer mode*>
The inverter current $i_p$ corresponds with $i_m$ at $t = t_5$. Then the current $i_{D7}$ through $\mathrm{D_7}$ naturally decays to zero owing to the effect of $L_s$, thereby ZCS turn-off operation can be realized in $\mathrm{D_7}$. After the moment, the power is delivered from $V_{in}$ to the load $R_o$ and the circuit operations get into the negative half cycle. At this time, $i_p$ is denoted as

$$i_p(t) = \frac{V_{in} - aV_o}{L_s}(t - t_5) + i_p(t_5). \quad (12)$$

## III. Analysis and Design of Soft-Switching Range

The primary-side inverter voltage and current waveforms of the conventional ZVS PPS-PWM dc-dc converter and the proposed soft-switching SPS-PWM dc-dc converter are depicted in Figs. 10 and 11, respectively. Note in those figures that the time origin $t_o$ is set to be 0 for simplifying the explanations below.

The primary-side inverter peak current $i_p(0)$ of both PPS-PWM and SPS-PWM dc-dc converters is generally expressed as

$$i_p(0) = i_{mp} + \frac{I_o}{a}. \quad (13)$$

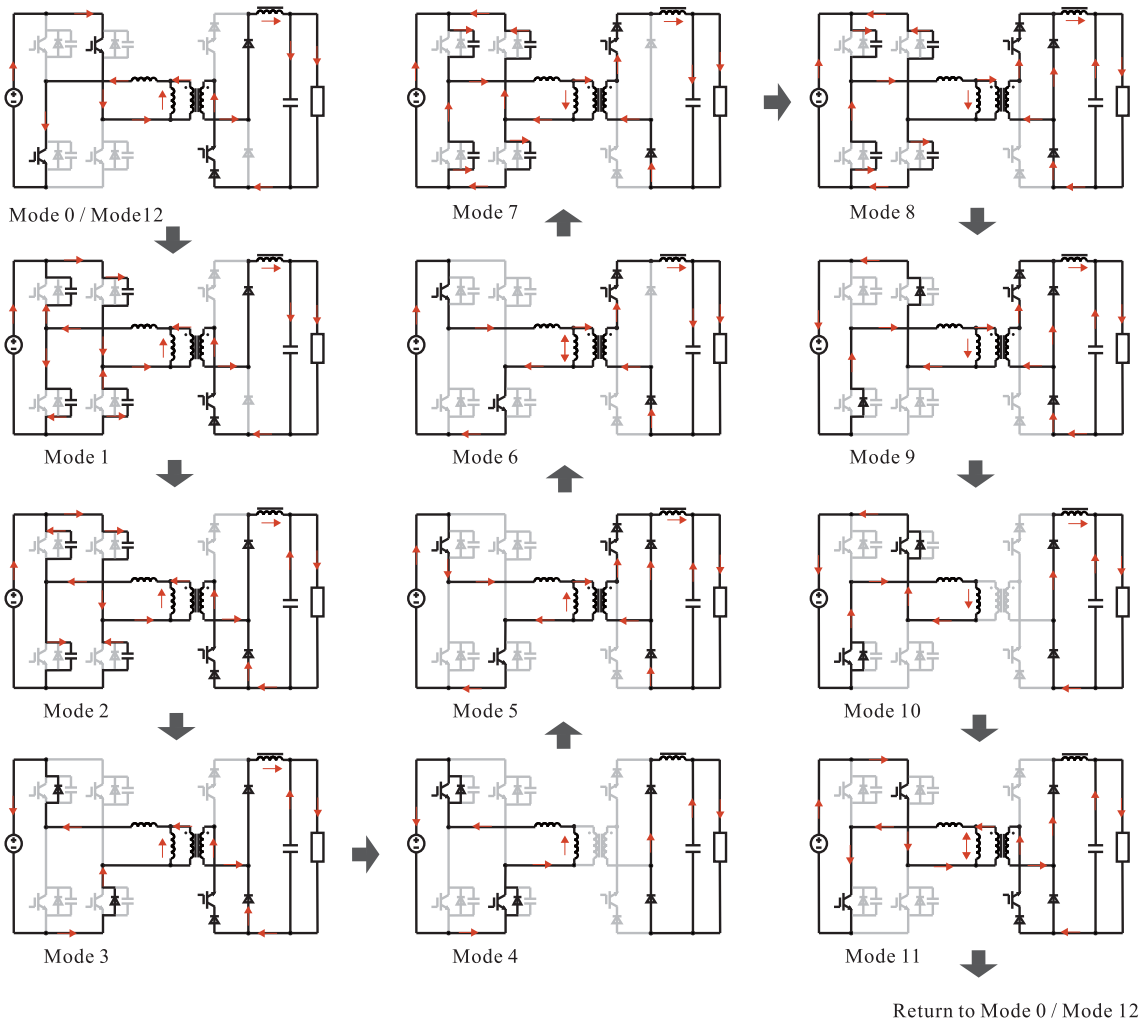


Fig. 9. Mode transitions and switching-mode equivalent circuits during one switching cycle.

From (13), $i_p(0)$ depends on the load current $I_o$ and the peak value of magnetizing current $i_{mp}$ as portrayed in Fig. 4. The peak value of magnetizing current in the conventional ZVS PPS-PWM dc-dc converter is defined from Fig. 10 as

$$i_{mp} = \frac{V_{in}}{2(L_s + L_m)} \cdot \left( \frac{T}{2} - t_\phi \right). \tag{14}$$

Therefore, ZVS operations in the primary-side active switches of the PPS-PWM dc-dc converter can not be achieved in the light load range due to the reduction of the magnetic energy.

On the other hand, the peak value of magnetizing current $i_{mp}$ in the proposed soft-switching dc-dc converter is load-independent. Therefore, $i_{mp}$ corresponds with the minimum value of the HF full-bridge inverter current $i_p$ for no load as indicated in Fig. 11.

The peak value of magnetizing current $i_{mp}$ herein can be derived by referring to Fig. 11 as

$$i_{mp} = i_m(T/2) = \frac{V_{in}}{L_s + L_m} \cdot \frac{T}{2} + i_m(0). \tag{15}$$

Since the periodical waveform condition $i_m(0) = -i_m(T/2)$ can be established, the peak value of magnetizing current $i_{mp}$ can be determined by deforming (15) as

$$i_{mp} = \frac{V_{in}}{2(L_s + L_m)} \cdot \frac{T}{2}. \tag{16}$$

It can be known from (13) that $i_p(0)$ of the proposed soft-switching dc-dc converter is constantly larger than $i_{mp}$ which is the load independent value. Therefore, ZVS operations can be achieved in the primary-side active switches of the proposed soft-switching dc-dc converter from no load to full load range by properly designing $i_{mp}$.

The on-intervals of secondary-side active switches $\mathrm{Q}_5$ and $\mathrm{Q}_6$ should be extended to $50\,\%$ to ensure the ZCS operations as shown in Fig. 12, which implies no dead time exists in the gate-pulse timings between $\mathrm{Q}_5$ and $\mathrm{Q}_6$. The extended duration $t_{ex}$ in the gate signals for $\mathrm{Q}_5, \mathrm{Q}_6$ and the dead time $t_{d1}$ of the primary-side active switches are required to satisfy the condition $t_{d1} \geq t_{ex}$.

All of the on-interval $T/2$ in Fig. 12 excluding the dead time $t_{d1}$ of the primary-side active switches is utilized for ZVS in the primary-side and ZCS in the secondary-side, then the soft-switching range index $K$ of the proposed dc-dc converter is defined as

$$K = \frac{T/2 - t_{ex}}{T/2}. \tag{17}$$

The magnetizing inductance $L_m$ is defined from (4) and (16)

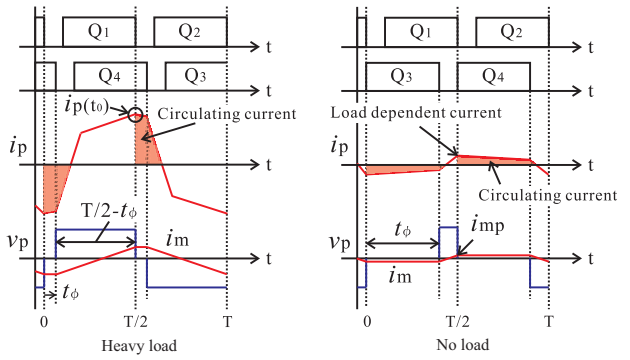


Fig. 10. Primary-side voltage and current waveforms of HF transformer in the conventional ZVS PPS-PWM dc-dc converter ($t_\phi$: phase-shift interval).

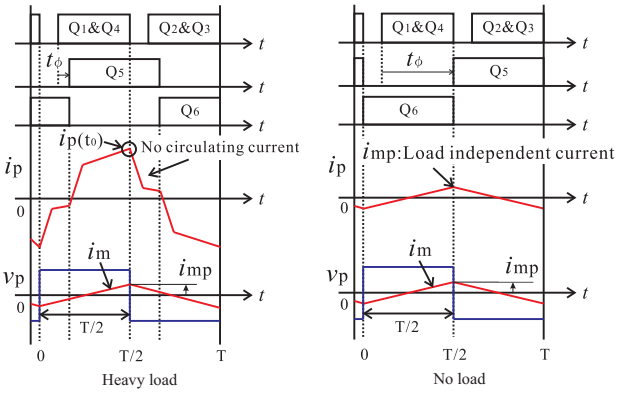


Fig. 11. Primary-side voltage and current waveforms of HF transformer in the proposed soft-switching SPS-PWM dc-dc converter ($t_\phi$: phase-shift interval).

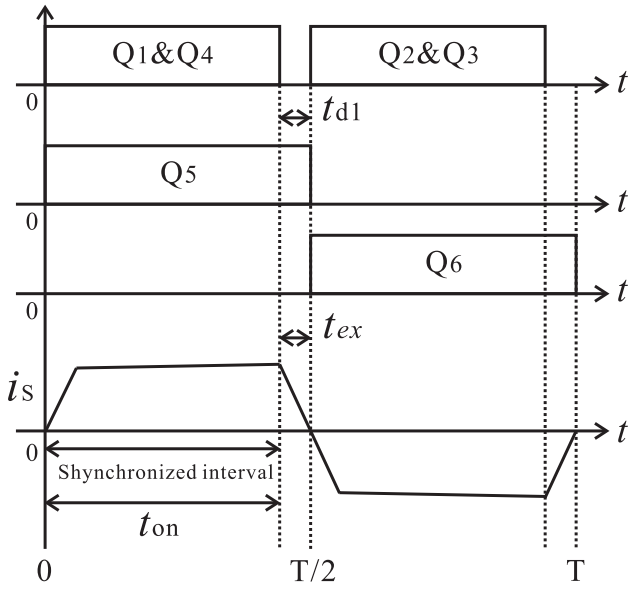


Fig. 12. Gate pulses sequences for the primary-side ZVS and secondary-side ZCS operations for the full load condition (no phase-shifting: $t_\phi = 0$).

under the conditions of $i_m(t_0) = i_m(0) = i_{mp}$ as

$$L_m = \frac{1}{4} \cdot \sqrt{\frac{L_s}{C_r}} \cdot \left(\frac{T}{2}\right) - L_s. \tag{18}$$

The HF inverter current $i_p(T/2)$ necessary for guaranteeing ZVS operations under no load condition is redefined by using

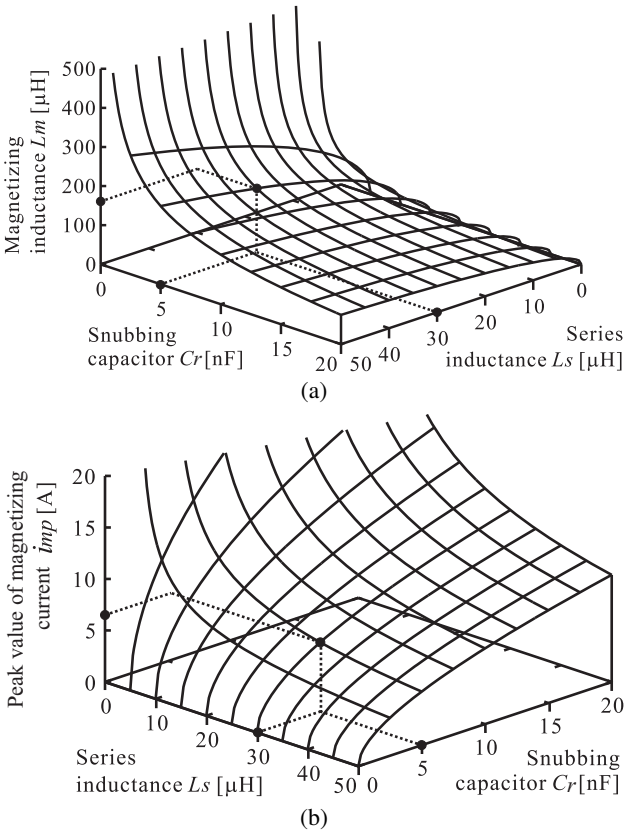


Fig. 13. Relationships of the HF transformer parameters ($V_{in} = 260$ V, $f_s = 50$ kHz): (a) magnetizing inductance $L_m$, (b) peak magnetizing current $i_{mp}$.

(4) as

$$i_p(T/2) = i_{mp} = \frac{2V_{in}}{\sqrt{L_s/C_r}}. \tag{19}$$

From (18) and (19), the variations of the magnetizing inductance $L_m$ in the HF transformer parameter with respect to the series inductor $L_s$ are shown in Fig. 13. As can be seen in Fig. 13 (a), the magnetizing inductance $L_m$ rises gradually as the series inductor $L_s$ increases. Therefore, the peak value of magnetizing current $i_{mp}$ is reduced as depicted in Fig. 13 (b). The series inductor $L_s$ is expressed on the basis of (18) by defining the inductance ratio $\zeta = L_m/L_s$ as

$$L_s = \frac{1}{16C_r\,(1+\zeta)^2} \cdot \left(\frac{T}{2}\right)^2. \tag{20}$$

Eq. (20) indicates the series inductor $L_s$ changes in accordance with the setting value of inductance ratio $\zeta$.

Since the dead time of the proposed soft-switching SPS-PWM dc-dc converter is $t_{d1} \geq t_{ex}$, the soft-switching range index $K$ in (17) is rewritten by using (9) and (20) as

$$K = 1 - \frac{aI_o}{V_{in}} \cdot \frac{1}{16C_r\,(1+\zeta)^2} \cdot \left(\frac{T}{2}\right). \tag{21}$$

The soft-switching range index $K$ is analytically depicted in Fig. 14. It can be understood from Fig. 14 that the soft-switching range depends on the dc input voltage $V_{in}$, lossless snubbing capacitor $C_r$, load current $I_o$, and the inductance ratio $\zeta$. In Fig. 14, $L_s$ decreases if the soft-switching range is large, consequently $i_{mp}$ increases as expressed by (19).

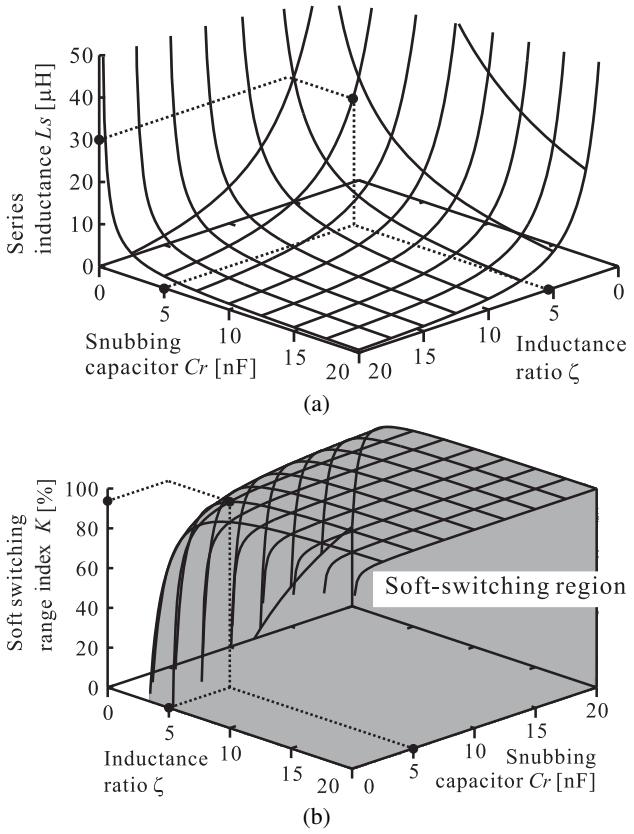


Fig. 14. Characteristics of soft-switching range with relevant circuit parameters ($V_{in} = 260$ V, $f_s = 50$ kHz): (a) series inductance $L_s$, (b) soft-switching range index $K$.

Therefore, the peak value of magnetizing current $i_{mp}$ should be designed as small as possible because the conduction losses related to the transitional interval of Mode 4 increase in accordance with the rise of $i_{mp}$.

## IV. Analysis of SPS-based Output Power Regulations

The output power characteristics with the phase shift angle $\phi$ (phase shift interval $t_\phi$) can be expressed on the basis of the primary-side referred equivalent circuits as shown in Fig. 15.

By assuming the time origin $t_0 = 0$ for simplicity, the primary-side inverter current $i_p$ can be specified for each interval in Fig. 15 under the condition by using (3), (8), (10) and (12) as

$$i_{p1}(t) = \frac{V_{in}}{L_s}(t) + i_p(0) \tag{22}$$

$$i_{p2}(t) = \frac{V_{in}}{L_s}\left(t + \frac{aV_o}{V_{in}}t_3\right) + i_p(0) \tag{23}$$

$$i_{p3}(t) = \frac{V_{in}}{L_s}\left\{t - \frac{1}{1+1/\zeta}(t_4 - t_3)\right\} + i_p(0) \tag{24}$$

$$i_{p4}(t) = \frac{V_{in}}{L_s}\left\{\left(1 - \frac{aV_o}{V_{in}}\right)t + \frac{aV_o}{V_{in}} - \frac{1}{1+1/\zeta}(t_4 - t_3)\right\} + i_p(0) \tag{25}$$

By proving the periodical waveform condition $i_p(T/2) = -i_p(t_0)$, combination of (22) and (25) yields $i_p(t_0)$ as

$$i_p(t_0) = \frac{V_{in}}{2L_s}\left\{\frac{1}{1+1/\zeta}(t_4 - t_3) - \left(1 - \frac{aV_o}{V_{in}}\right)\cdot\frac{T}{2} - \frac{aV_o}{V_{in}}\right\} \tag{26}$$

Then, the ampere–second values of each time interval in Fig. 15 are expressed by

$$\begin{aligned} S_1 &= \int_{t_o}^{t_3} i_{p1}(t)dt \\ &= \frac{t_1}{2L_s}\left[V_{in}t_1 + V_{in}\left\{\frac{1}{1+1/\zeta}(t_4 - t_3) - \frac{T}{2}\right\}\right. \\ &+ \left. aV_o\left(\frac{T}{2} - t_5\right)\right] \end{aligned} \tag{27}$$

$$\begin{aligned} S_2 &= \int_{t_3}^{t_4} i_{p2}(t)dt \\ &= \frac{t_4 - t_3}{2L_s}\left[\frac{2}{1+1/\zeta}V_{in}(t_4 + t_3) - \frac{V_{in}T}{2}(t_4 - t_3)\right. \\ &+ \left. aV_o\left(\frac{T}{2} - t_5\right)\right] \end{aligned} \tag{28}$$

$$\begin{aligned} S_3 &= \int_{t_4}^{t_5} i_{p3}(t)dt = \frac{t_5 - t_4}{2L_s}\left[V_{in}(t_5 + t_4)\right. \\ &- \left. V_{in}\left\{\frac{1}{1+1/\zeta}(t_4 - t_3) + \frac{T}{2}\right\} + aV_o\left(\frac{T}{2} - t_5\right)\right] \end{aligned} \tag{29}$$

$$\begin{aligned} S_4 &= \int_{t_5}^{t_{T/2}} i_{p4}(t)dt = \frac{T/2 - t_5}{2L_s}\left[(V_{in} - aV_o)\left\{\left(\frac{T}{2}\right) + t_5\right\}\right. \\ &- \left. V_{in}\left\{\frac{1}{1+1/\zeta}(t_4 - t_3) + \frac{T}{2}\right\} + aV_o\left(\frac{T}{2} + t_5\right)\right] \end{aligned} \tag{30}$$

The ampere–second value $S_o = \sum_{k=1}^{4} S_k$ of the HF transformer primary-side current $i_p$ for half a switching cycle can be obtained from (27)–(30) as

$$\begin{aligned} S_o &= \frac{1}{2L_s}\left[V_{in}\cdot\frac{1}{1+1/\zeta}(t_4 - t_3)\left(t_4 + t_3 - \frac{T}{2}\right)\right. \\ &+ \left. aV_o\cdot t_5\left(\frac{T}{2} - t_5\right)\right] \end{aligned} \tag{31}$$

By giving the time conditions of $t_4 = t_3 + t_\phi$, $t_5 = 2t_3 + t_\phi$ and neglecting power losses of the dc-dc converter, the output power $P_o$ of the proposed soft-switching dc-dc converter is defined as

$$\begin{aligned} P_o &= V_{in}\overline{i_p} = 2V_{in}\cdot\frac{S_o}{T} \\ &= \frac{V_{in}}{TL_s}\left[V_{in}\cdot\frac{1}{1+1/\zeta}\cdot t_\phi\left(2t_3 + t_\phi - \frac{T}{2}\right)\right. \\ &- \left. aV_o(2t_3 + t_\phi)\left(2t_3 + t_\phi - \frac{T}{2}\right)\right] \end{aligned} \tag{32}$$

Fig. 16 illustrates the output power vs. phase shift angle characteristics by the computer-aided theoretical analysis based on (32) and the simulations under the open and closed loop control schemes, respectively. The simulation circuit

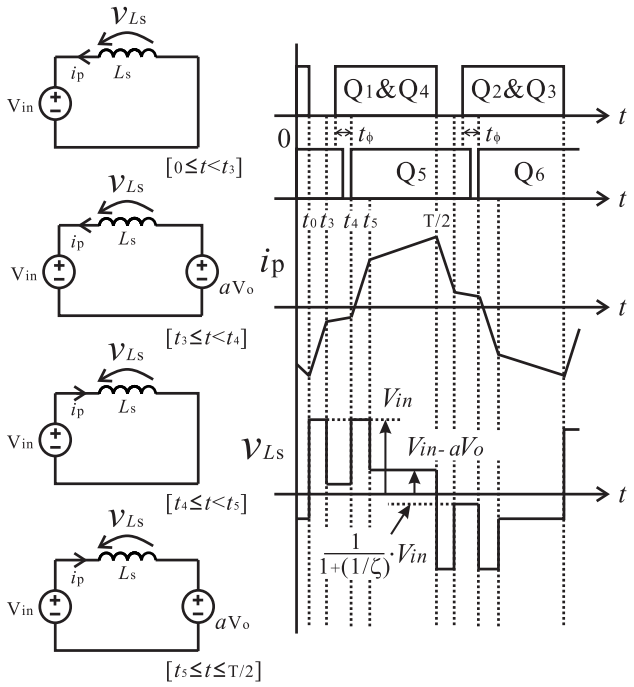


Fig. 15. Primary-side referred simplified equivalent circuits and waveforms for a half switching cycle.

TABLE I
SIMULATION CIRCUIT PARAMETERS.

| Parameter *Symbol* | Value unit |
|---|---|
| DC input voltage rating $V_{in}$ | 260 V |
| Output power rating $P_{o,rating}$ | 1 kW |
| Switching frequency $f_s$ | 50 kHz |
| Loss-less snubbing capacitors $C_r(C_1 - C_4)$ | 3 nF |
| Rated load resistance $R_o$ | 40 Ω |
| Output smoothing capacitor $C_o$ | 1500 μF |
| Output smoothing inductor $L_o$ | 620 μH |
| HF transformer turns ratio $a = N_p/N_s$ | 8 / 8 |
| HF transformer transformer magnetizing inductance $L_m$ | 230 μH |
| HF transformer series inductance $L_s$ | 33 μH |

parameters are indicated in TABLE I. It can be confirmed in Fig. 16 that the proposed soft-switching SPS-PWM dc-dc converter can attain the power regulation from the full load to no load under the complete soft-switching operations. The simulation values well agree with the theoretical ones, thereby the validity of the analysis based on (32) is proven.

The output power and output voltage can be controlled by the small phase shift angle as depicted in Fig. 16(b), which indicates that the proposed soft-switching SPS-PWM dc-dc converter has a good response to the load variations.

## V. EXPERIMENTAL RESULTS AND DISCUSSIONS

### A. Specification of Experimental Prototype

The switching performances and the steady-state characteristics of the proposed soft-switching SPS-PWM dc-dc converter are investigated in an experiment based on the laboratory prototype.

The schematic diagram of experimental circuit is shown in Fig. 17. The exterior appearances of laboratory prototype

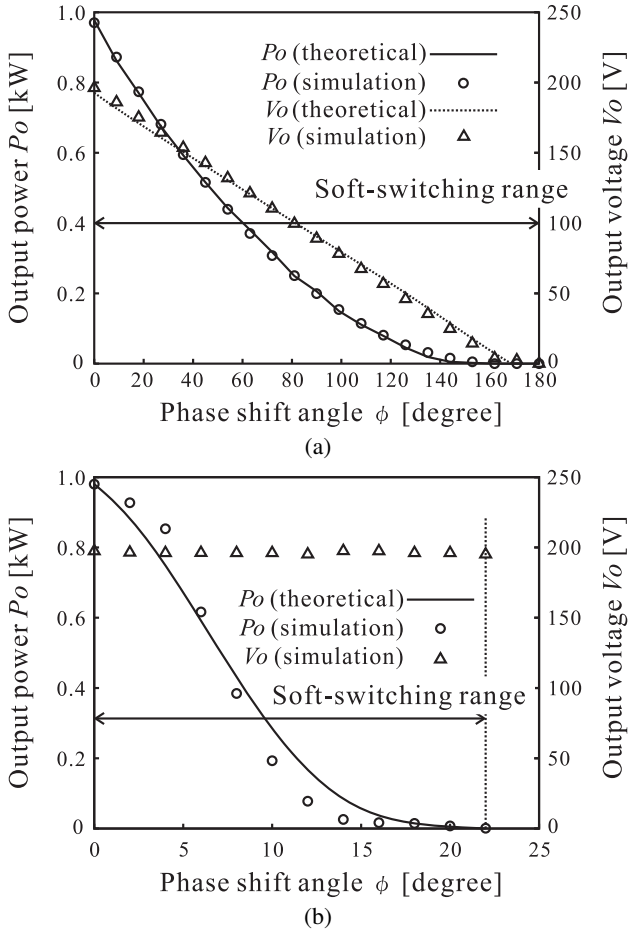


Fig. 16. Theoretical and simulation characteristics of output power and voltage vs. phase shift angle ($\zeta = 7$): (a) open loop, (b) closed loop control.

are depicted in Fig. 18. In this experiment, the laboratory prototype is designed as the preliminary step to be applied for the EV battery charging system, then an electric dc load is employed instead of battery packs for simplifying the experimental verifications as portrayed in Fig. 18 (a). The phase shift gate signals for $S_1$–$S_6$ are generated by using a phase shift PWM IC – *UCC3895*, and the closed loop control can be realized by a voltage PI controller. The primary-side active switches $Q_1$–$Q_4$ are implemented with High Speed IGBTs IXGN 60N60C2D1 while the secondary-side switches $Q_5$ and $Q_6$ are composed by combination of a high speed IGBT IXGN 60N60C2D1 and a fast recovery diode (FRD) module DSEI2x31-06C as depicted in Fig. 18 (b). In order to impose the reverse voltages into $D_5$ and $D_6$ properly, the antiparallel diodes-packed IGBTs are employed for $S_5$ and $S_6$ in the ZCS active rectifier.

The circuit parameters and specifications are illustrated in TABLE II.

### B. Converter Design Procedure

The design procedure of circuit parameters in the prototype is demonstrated by using the numerical example of rating values as follows: dc input voltage $V_{in} = 260$ V, output power rating $P_{o,rating} = 1$ kW, switching frequency $f_s = 50$ kHz, and rated load resistance $R_o = 40\,\Omega$.

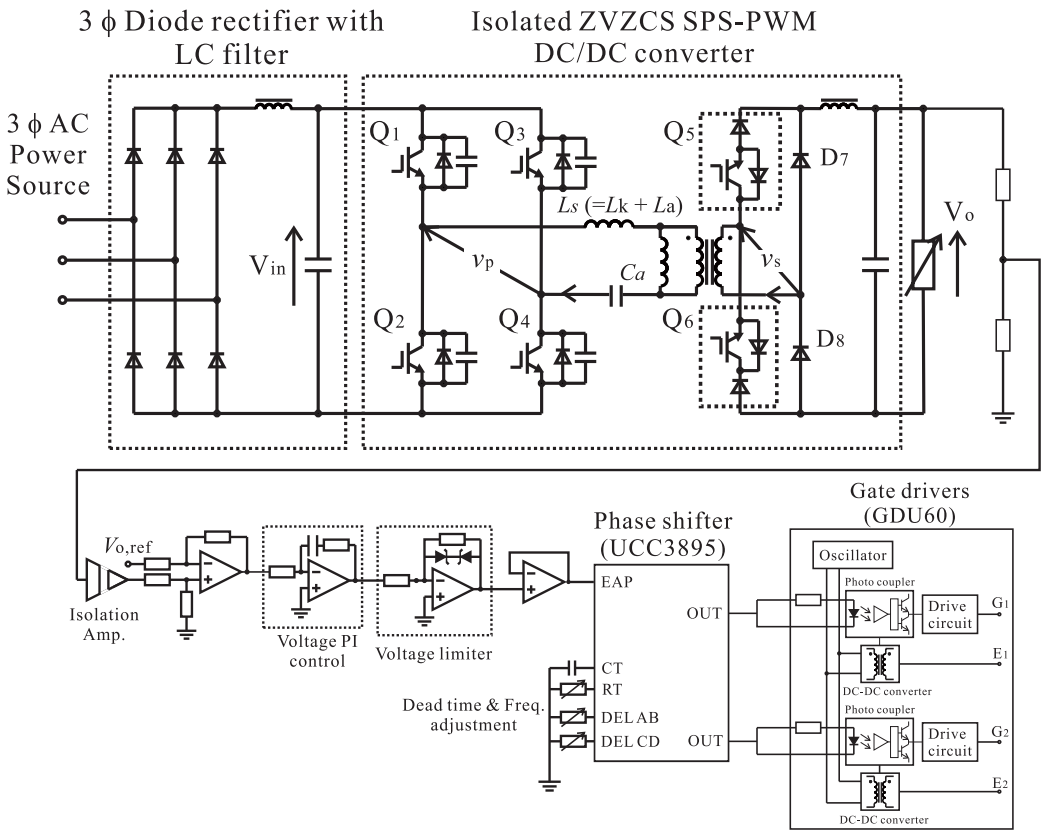


Fig. 17. Schematic diagram of laboratory prototype.

TABLE II
CIRCUIT PARAMETERS AND SPECIFICATIONS OF LABORATORY PROTOTYPE.

| Parameter *Symbol* | Value unit |
|---|---|
| DC input voltage rating $V_{in}$ | 260 V |
| Output power rating $P_{o,rating}$ | 1 kW |
| Switching frequency $f_s$ | 50 kHz |
| Loss-less snubbing capacitors $C_r(C_1 - C_4)$ | 3 nF |
| Auxiliary capacitor for DC magnetization protecting $C_a$ | 30 $\mu$F |
| Rated load resistance $R_o$ | 40 $\Omega$ |
| Output smoothing capacitor $C_o$ | 1500 $\mu$F |
| Output smoothing inductor $L_o$ | 620 $\mu$H |
| Additional series inductor $L_a$ | 30 $\mu$H |
| HF transformer turns ratio $a = N_p/N_s$ | 8 / 8 |
| HF transformer magnetizing inductance $L_m$ | 230 $\mu$H |
| HF transformer leakage inductance $L_k$ | 1.2 $\mu$H |
| HF transformer series inductance $L_s(= L_a + L_k)$ | 31.2 $\mu$H |

·$Q_1$–$Q_4$: IXYS IXGN60N60C2D1
·$Q_5$, $Q_6$: IXYS IXGN60N60C2D1 & DSEI2x31-06C
·$D_7$, $D_8$: IXYS DSEI2x31-06C

Assuming that the conduction losses, switching losses, and the equivalent series resistances (ESRs) of the input and output filters are neglected, the rating values of output voltage $V_o$ and current $I_o$ are determined by

$$V_o = \sqrt{P_{o,rating} \cdot R_o} = 200\,\mathrm{V}, \quad (33)$$

$$I_o = \sqrt{\frac{P_{o,rating}}{R_o}} = 5\,\mathrm{A}. \quad (34)$$

Accordingly, the peak value of magnetizing current $i_{mp}$ is set to be 5 A in order to achieve the ZVS operations of the primary-side active switches $Q_1$–$Q_4$ over the wide load range. When the $\Delta v/\Delta t$ values of $Q_1 - Q_4$ are given to be 2 kV/$\mu$s, the lossless snubbing capacitors $C_r$ are calculated by

$$C_r = \frac{i_{mp} + I_o/a}{2} \cdot \frac{\Delta t}{\Delta v} = 2.5\,\mathrm{nF}. \quad (35)$$

Using (4), the HF transformer series inductance $L_s$ including its leakage inductance $L_k$ can be determined as

$$L_s \geq \frac{4C_r {V_{in}}^2}{{i_{mp}}^2} = 27\,\mu\mathrm{H}. \quad (36)$$

Then, it is reasonable to select the additional inductor $L_a = 30\,\mu$H in series with the leakage inductance $L_k = 1.2\,\mu$H of the HF transformer. The HF inverter current $i_p$ is equal to the magnetizing current $i_m$ under the no load condition ($t_\phi = T/2$). Therefore, the HF inverter peak current $i_p(t_0)$ for no load condition corresponds with $i_{mp}$. Thus, $L_m$ can be obtained as

$$L_m = \frac{V_{in}}{2i_{mp}} \cdot \frac{T}{2} - L_s = 230\,\mu\mathrm{H}, \quad (37)$$

where $T$ denotes the interval of one switching cycle ($T = 1/f_s$).

The minimum dead time $t_{d1,min}$ of the primary-side active switches for no load condition can be determined as

$$t_{d1,min} = \frac{2C_r N_T V_{in}}{i_{mp}} = 0.26\,\mu\mathrm{s}. \quad (38)$$

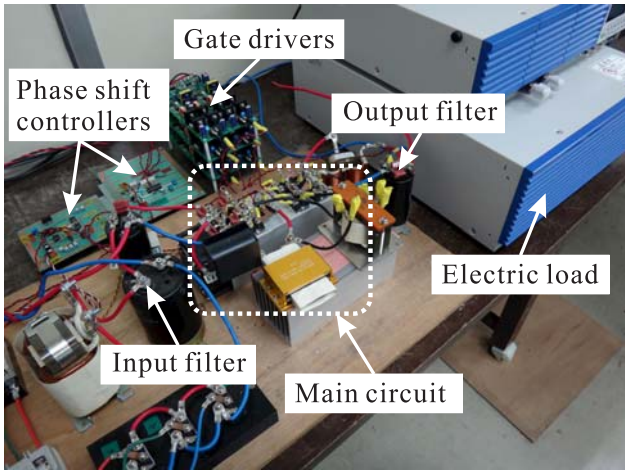


(a)

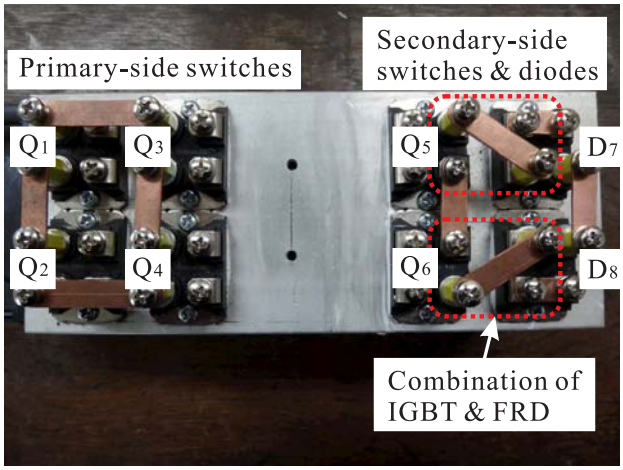


(b)

Fig. 18. Exterior appearance of 1 kW – 50 kHz laboratory prototype: (a) experimental circuit, (b) active switches and diodes implementations.

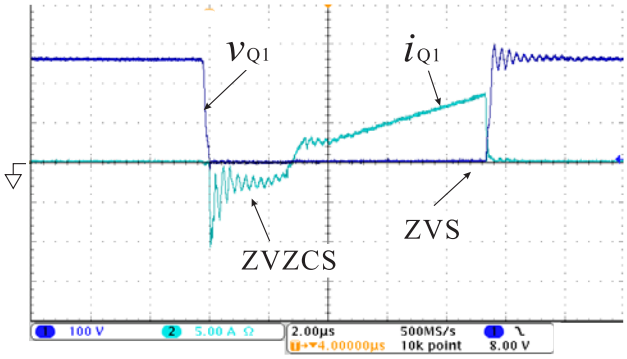


(a)

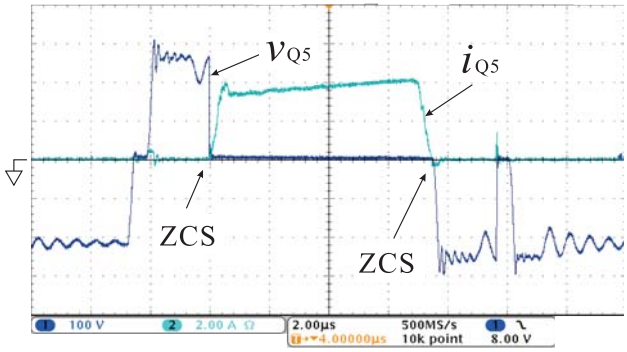


(b)

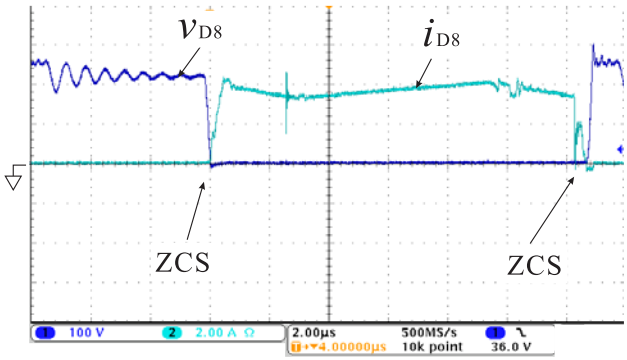


(c)

Fig. 19. Measured converter operating waveforms at $\phi = 36°$ and $P_o = 580$ W: (a) primary-side switch $Q_1$, (b) secondary-side switch $Q_5$, (c) secondary-side diode $D_8$ (100 V/div, 2 A/div, 2 $\mu$s/div).

The dead time $t_{d1}$ of the primary-side inverter is determined by considering $t_{ex}$ in (9) as

$$t_{d1} = \frac{aL_s}{V_{in}} I_o \cong 0.57\,\mu\text{s}. \tag{39}$$

In contrast, the dead time $t_{d2}$ of the secondary-side active rectifier is set to be $t_{d2} \cong 0$ as a minimum value according to the converter operating principle mentioned above.

### C. Switching Operations

The measured switching waveforms of the active switches and the rectifying diodes are depicted in Fig. 19 under the condition of $P_o = 580$ W and $\phi = 36°$. In addition, the corresponding voltage and current lissajous figures are indicated in Fig. 20. It can be actually confirmed from those results that ZVZCS turn-on and ZVS turn-off in the primary-side active switch $Q_1$, ZCS turn-on / off in the secondary-side active switch $Q_5$ and ZCS turn-on / off commutations in the rectifying diode $D_8$ can be actually attained, respectively.

The measured switching waveforms under the condition of light load power setting ($P_o = 60$ W, $\phi = 117°$) is illustrated in Fig. 21. In addition, the corresponding voltage and current lissajous figures are indicated in Fig. 22. It is clearly demonstrated in Figs. 21 and 22 that the proposed soft-switching SPS-PWM dc-dc converter can achieve the soft-switching operation even in the light load by designing the circuit parameters on the basis of the design guideline.

The voltage and current waveforms of the primary-side inverter and the secondary-side rectifier are demonstrated for the two sets of load conditions in Figs. 23 and 24. It can be confirmed from the measured waveforms that circulating currents both of the primary and secondary-side circuits are well reduced in the proposed dc-dc converter over the wide load range. Thus, the effectiveness of the ZCS active rectifier-assisted SPS-PWM scheme is actually verified.

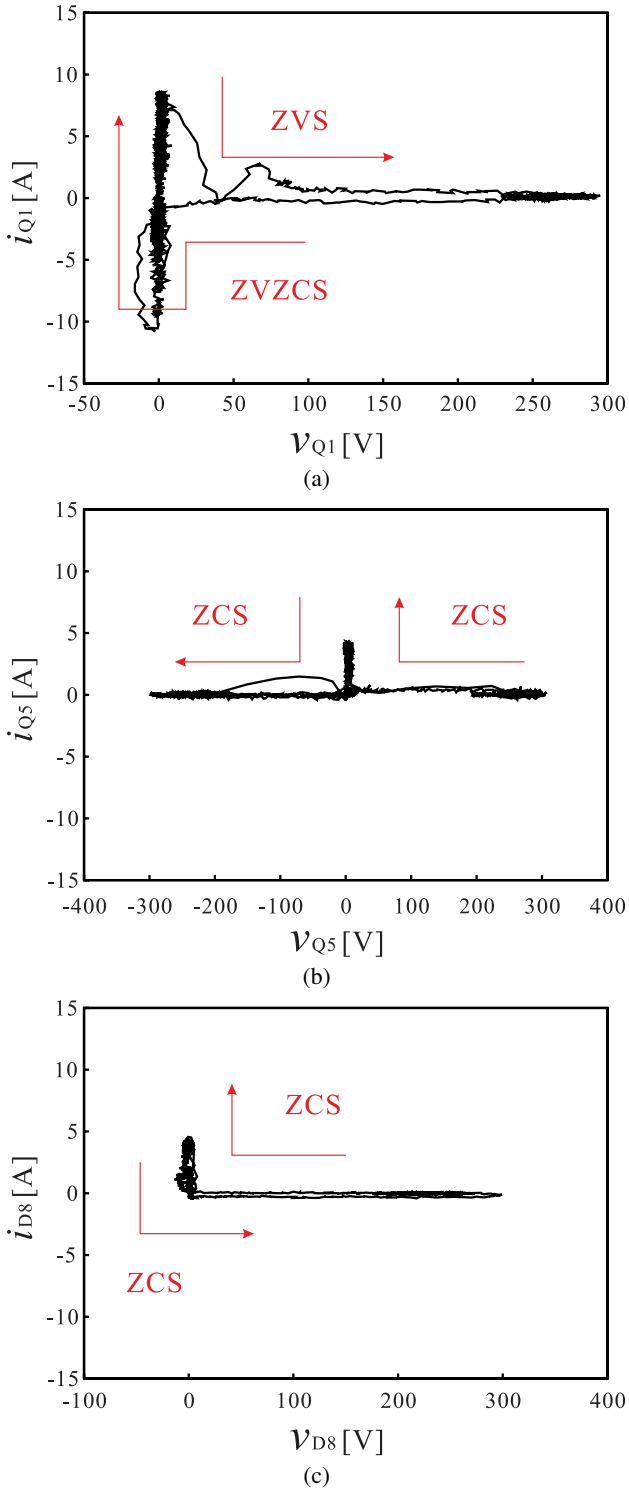


Fig. 20. Active switches and diodes lissajous figures at $\phi = 36^\circ$ and $P_o = 580$ W: (a) primary-side switch $Q_1$, (b) secondary-side switch $Q_5$, (c) secondary-side diode $D_8$.

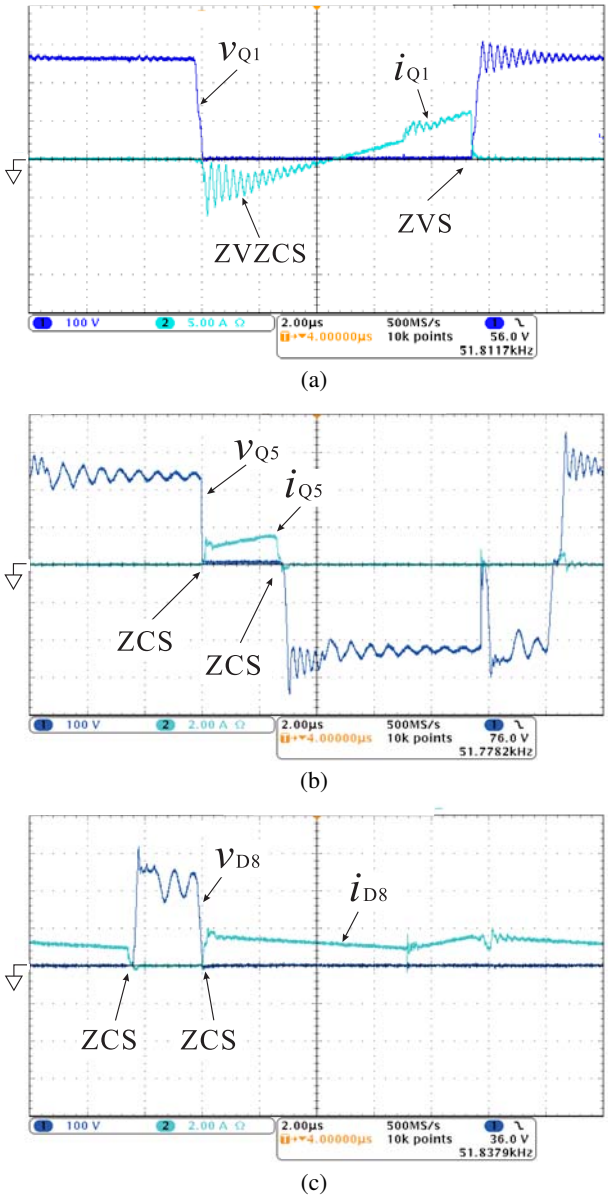


Fig. 21. Measured converter operating waveforms at $\phi = 117^\circ$ and $P_o = 60$ W: (a) primary-side switch $Q_1$, (b) secondary-side switch $Q_5$, (c) secondary-side diode $D_8$ (100 V/div, 2 A/div, 2 $\mu$s/div).

### D. Steady-Sate Characteristics

The characteristics of the output power and voltage vs. phase shift angle are illustrated in Fig. 25 for the open loop and closed loop controls, respectively.

The wide-range output power and voltage regulations as well as the full-range soft switching operations of the proposed soft-switching SPS-PWM dc-dc converter can be observed in Fig. 25 (a) under the condition of variable output voltage. The experimental characteristics well agree with the theoretical and simulation ones in Fig. 16(a).

The output power and voltage regulation characteristics with the closed loop control are provided in Fig. 25 (b). The output power and voltage can be widely controlled with the relatively small variation of the phase shift angle under the condition of constant output voltage. The experimental characteristics well agree with the theoretical and simulation ones in Fig. 16(b).

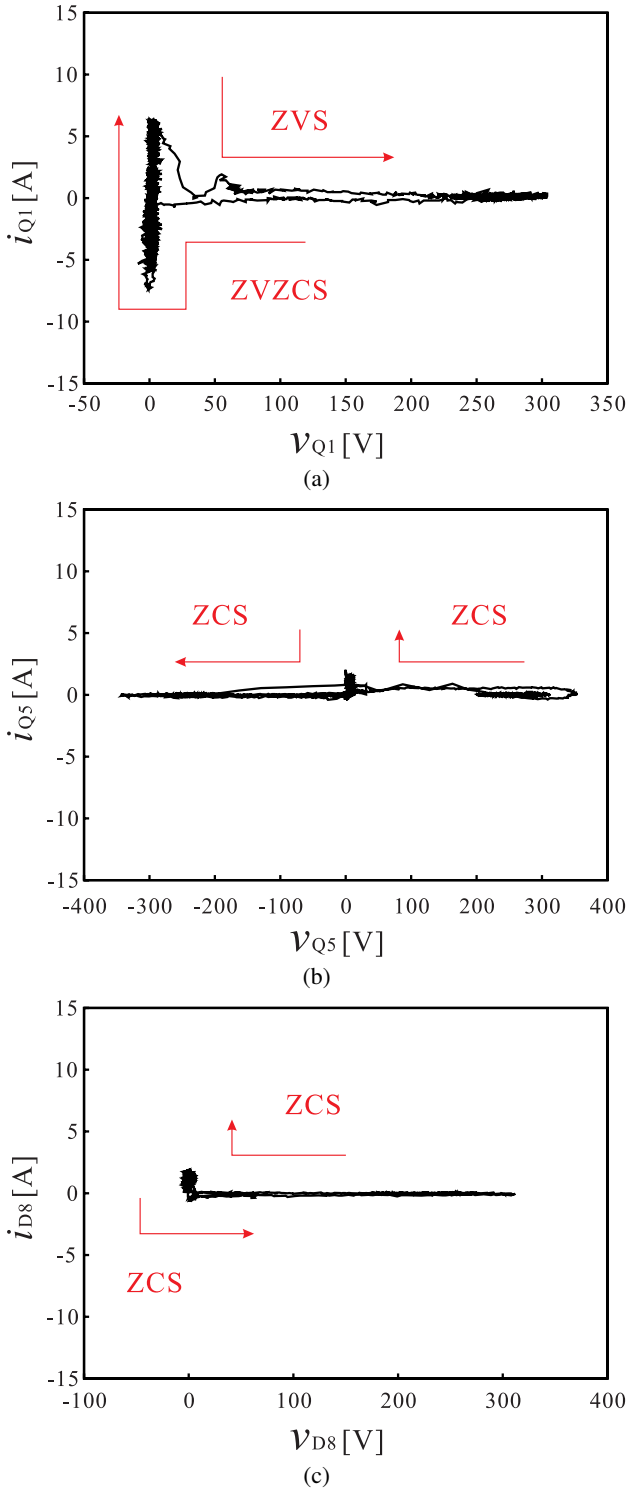


Fig. 22. Active switches and diodes lissajous waveforms at $\phi = 117\,^\circ$ and $P_o = 60$ W: (a) primary-side switch $Q_1$, (b) secondary-side switch $Q_5$, (c) secondary-side diode $D_8$.

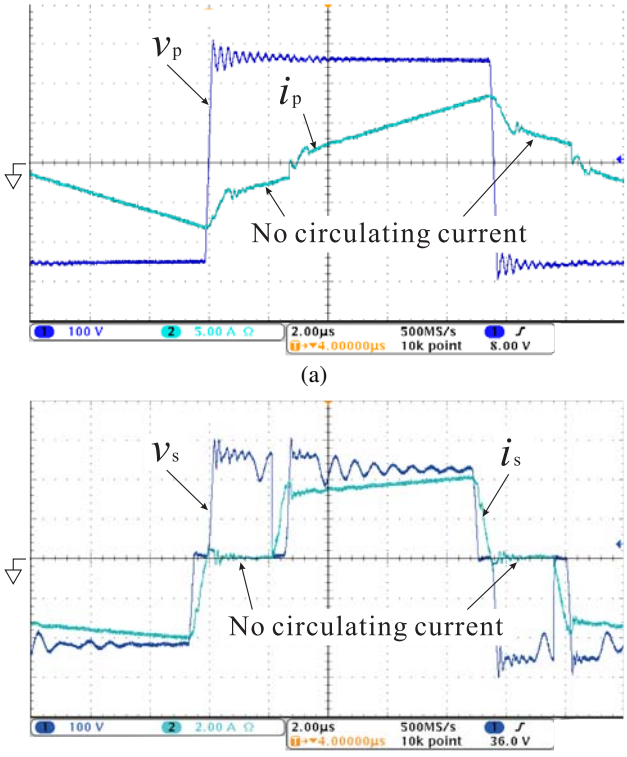


Fig. 23. Voltage and current waveforms of HF transformer windings at $\phi = 36\,^\circ$ and $P_o = 580$ W : (a) primary-side, (b) secondary-side (100 V/div, 2 A/div, 2 $\mu$s/div).

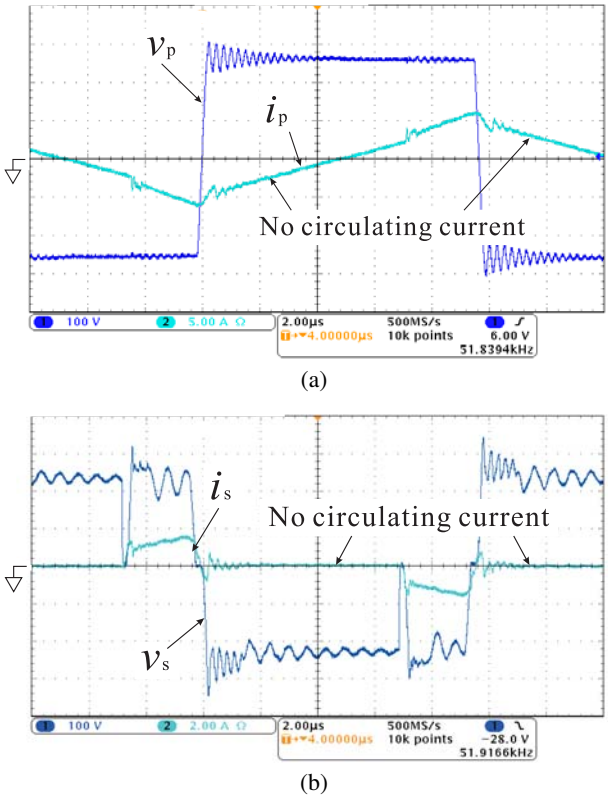


Fig. 24. Voltage and current waveforms of HF transformer windings at $\phi = 117\,^\circ$ and $P_o = 60$ W : (a) primary-side, (b) secondary-side (100 V/div, 2 A/div, 2 $\mu$s/div).

In Fig. 25, the output power and voltage regulation characteristics show a linearity with the phase shift angle, accord-

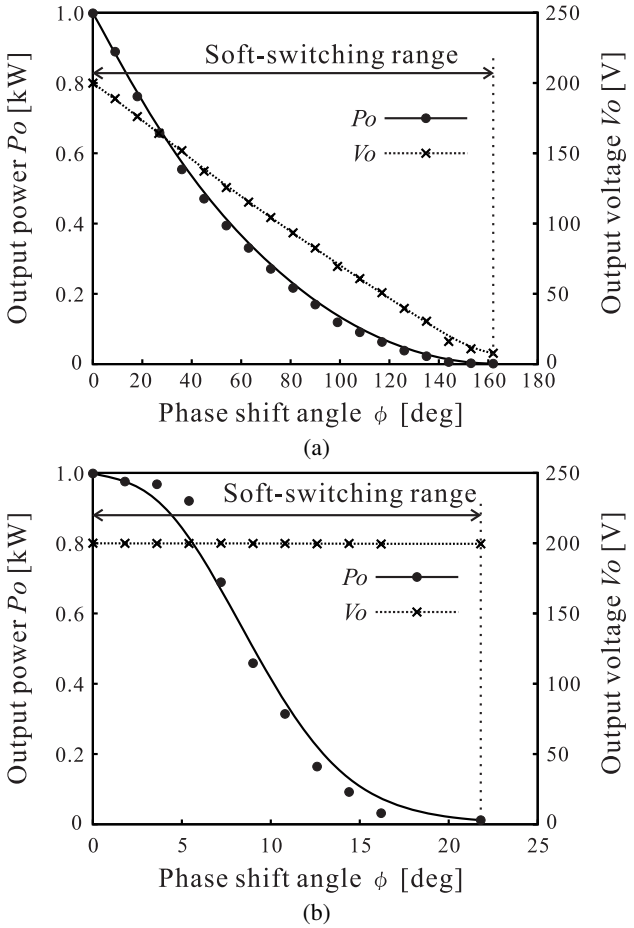


Fig. 25. Experimental characteristics of output power and out voltage vs. phase shift angle: (a) open loop, (b) closed loop control.

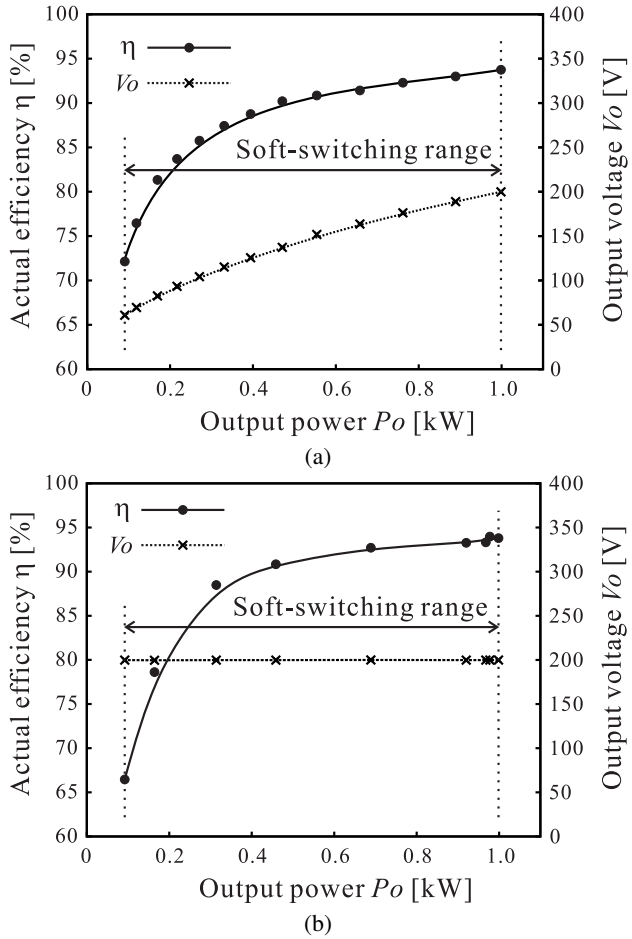


Fig. 26. Power conversion efficiency of the proposed dc-dc converter prototype: (a) open loop, (b) closed loop control.

ingly the controller can be configured by the relatively simple scheme. Moreover, the proposed soft-switching SPS-PWM dc-dc converter can operate over the wide load range under the soft-switching conditions.

The actual conversion efficiencies of the prototype treated herein are illustrated in Fig. 26. The soft-switching operations of the active switches and diodes are actually confirmed over the entire load range by the experimental data as indicated in Fig. 26. It can be confirmed that over 90 % efficiency can be obtained from the middle to heavy load conditions in the laboratory prototype.

The performances of the proposed soft-switching SPS-PWM dc-dc converter for the typical CCCV battery charging operations which are modeled with an electric load are shown in Fig. 27. The actual control range denotes the practical operating range when the low voltage limit of battery is assumed to be 75 % (150 V) of the fully-charged voltage (200 V). In the CC region, the output voltage increases linearly by decreasing the phase shift angle $\phi$. Once the output voltage approaches the rated value, the output current is regulated by gradually increasing $\phi$ and the CV condition keeps until the fully-charged state. Thus, the effectiveness of the proposed soft-switching SPS-PWM dc-dc converter as a battery charger is preliminary demonstrated herein. The soft switching operations can be confirmed in the whole region of the CCCV battery charging pattern.

### *E. Power Loss Analysis*

The power loss analysis of the prototype is depicted in Fig. 28.

The switching power losses of each power device are actually reduced among the power loss breakdowns from light to heavy load conditions. Thus, the effect of employing the soft-switching technologies is clearly confirmed herein.

On the other hand, the conduction power losses of each power device and the copper loss of HF transformer dominate the main part of the total breakdown. In particular, the conduction power losses of the secondary-side active switches $Q_5$ and $Q_6$ exhibit a relatively high profile in the heavy load condition. This is due to the structure of $Q_5$ and $Q_6$ which are composed of the series connection of discrete IGBT and FRD, respectively. Therefore, applying a one-chip reverse conduction blocking IGBT (RB-IGBT) with fast reverse recovery characteristics for the secondary-side active switches will be an effective solution for further reducing the conduction power losses of the ZCS active rectifier, although it is still in the developing stage.

As an actual EV battery charger, the proposed soft-switching SPS-PWM dc-dc converter can be extended for the multi-phase circuit configuration for higher power level as illustrated in Fig. 29. The output current ripple frequency can be increased by triple in the multi-phase topology, thereby the filter size just after the secondary-side rectifier can be effectively

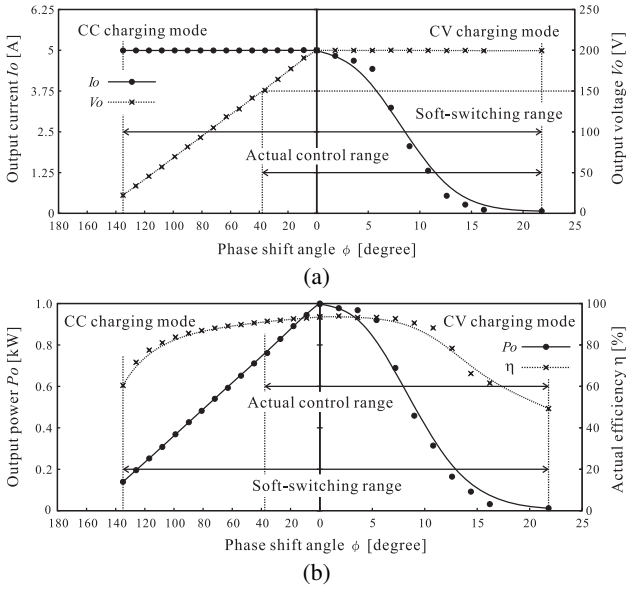


Fig. 27. Converter performances for CCCV operation: (a) output voltage and current vs. phase-shift angle, (b) output power and efficiency vs. phase-shift angle.

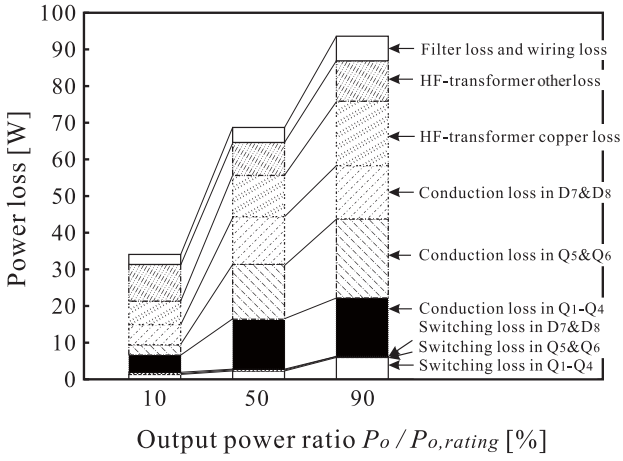


Fig. 28. Power loss analysis for various load conditions.

reduced.

## VI. Conclusions

A new prototype of the secondary-side phase shift (SPS) PWM soft-switching dc-dc converter applicable for EV battery chargers has been presented in this paper. The wide-range soft-switching operations of the proposed soft-switching SPS-PWM dc-dc converter have been clarified with the theoretical analysis and simulation results, and then the circuit design guidelines have been originally described, which contributes for engineers in actually developing the soft-switching dc-dc converter proposed herein. In addition to these, the output power regulation based on the SPS scheme has been theoretically analyzed, exhibiting its wide range output power and output voltage regulations capability.

The performances of the proposed soft-switching dc-dc converter are evaluated in an experiment using the 1 kW-50 kHz laboratory prototype. It can be actually demonstrated

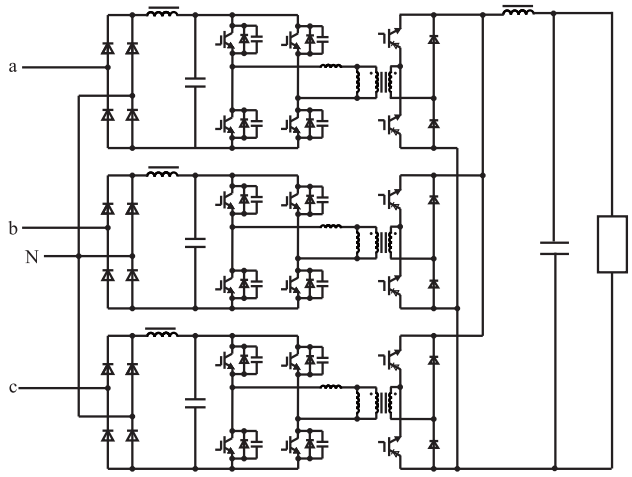


Fig. 29. Three-phase circuit topology of the proposed soft-switching SPS-PWM dc-dc converter with high-speed RB-IGBTs for higher power level.

that the wide-range soft-switching can be attained from the heavy load to light load. In addition, it has been confirmed that the output power can be controlled from full load to no load with a relatively small variation of the phase shift angle. Those unique characteristics provide high performances for the dc-dc converter applied for the EVs/PHEVs battery chargers.

The actual performances of the proposed soft-switching dc-dc converter has also been demonstrated for the CCCV battery charging pattern which is modeled by an electric dc load in the laboratory prototype. The relevant experimental results have made it clear that the wide-range output voltage and current regulations can be achieved in the proposed soft-switching dc-dc converter. Furthermore, the power loss analysis of the laboratory prototype has indicated that the conduction loss of the secondary-side power devices should be minimized, then the conversion efficiency might be improved much more by applying the one-chip IGBT with fast recover capability.

The extended three-phase power converter topology has been newly demonstrated for higher power EV battery charges as a next-stage research challenge of the proposed soft-switching dc-dc converter.

## References

[1] A. Emadi, Y. J. Lee, and K. Rajashekara, "Power electronics and motor drive in electric, hybrid electric, and plug-in hybrid electric vehicles", *IEEE Trans. Ind. Electron.*, vol.55, no.6, pp.2237–2245, Jun. 2008

[2] I-O. Lee and G-W. Moon, "Phase-shifted PWM converter with a wide ZVS range and reduced circulating current," *IEEE Trans. Power Electron.*, vol.28, no.2, pp.908-919, Feb. 2013.

[3] B. Gu, J.-S. Lai, N. Kees, and C. Zheng, "Hybrid-switching full-bridge dc-dc converter with minimal voltage stress of bridge rectifier, reduced circulating losses, and filter requirement for electric vehicle battery charges," *IEEE Trans. Power Electron.*, vol.28, no.3, pp.1132–1144, Mar. 2013.

[4] M. Narimani and G. Moschopoulos, "A new dc/dc converter with wide-range ZVS and reduced circulating current," *IEEE Trans. Power Electron.*, vol.28, no.3, pp.1265–1273, Mar. 2013.

[5] M. Pahlevaninezhad, P. Das, J. Drobnik, P.-K. Jain, and A. Bakhshai, "A novel ZVZCS full-bridge dc/dc converter used for electric vehicles," *IEEE Trans. Power Electron.*, vol.27, no.6, pp.2752–2769, Jun. 2012.

[6] D-S. Gautam, and A-K-S. Bhat, "A comparison of soft-switched dc-to-dc converters for electrolyzer application," *IEEE Trans. Power Electron.*, vol.28, no.1, pp.54–62, Jan. 2013.

[7] I.-H. Cho, K.-M. Cho, J.-W. Kim, and G.-W. Moon, "A new phase-shifted full bridge converter with maximum duty operation for server power system," in *Proc. International Power Electronics and Motion Control Conference ECCE Asia* (IPEMC), May 2011, pp.1278–1285.

[8] A. Bellini, S. Bifaretti, and V. Iacovone, "A zero-voltage transition full bridge dc-dc converter for photovoltaic applications," in *Proc. Intl. Symp. Power Electron., Electr. Drives, Autom. Motion*, Jun. 2010, pp.448–453.

[9] J. Dudrik and N-D. Trip, "Soft-switching PS-PWM dc-dc converter for full-load range applications," *IEEE Trans. Power Electron.*, vol.57, no.8, pp.2807–2814, Aug. 2010.

[10] W.J. Lee, G-E Kim, G-W Moon, and S-K Han, "A new phase-shifted full-bridge converter with voltage-doubler-type rectifier for high-efficiency PDP sustaining power modules," *IEEE Trans. Ind. Electron.,* vol.55, no.6, pp.2450–2458, Jun. 2008.

[11] U.Badstuebner, J.Biela, B.Faesssler, D.Hoesli, and J.W. Kolar, "An optimized 5 kW 147 W/in$^3$ telecom phase-shift dc-dc converter with magnetically integrated current doubler," in *Proc. IEEE Applied Power Electronics Conference and Expositions* (IEEE APEC), Feb. 2009, pp.21–27.

[12] A. K. Jain, R. Ayyanar, "PWM control of dual active bridge: comprehensive analysis and experimental verification," *IEEE Trans. Power Electron.,* vol.26, no.4, pp.1215–1227, Apr. 2011.

[13] A. F. Bakan, N. Altintas, and I. Aksoy, "An improve PSFB PWM dc-dc converter for high-power and frequency applications," *IEEE Trans. Power Electron.,* vol.28, no.1, pp.64–74, Jan. 2013.

[14] H.S. Choi, J.W. Kim, and B.H. Cho, "Novel zero-voltage and zero-current-switching (ZVZCS) full-bridge PWM converter using coupled output inductor," *IEEE Trans. Power Electron.,* vol.17, no.5, pp.641–648, Sep. 2002.

[15] E.-S. Kim, K.-Y. Joe, M.-H. Kye, Y.-H. Kim, and B.-D. Yoon, "An improved soft-switching PWM FB dc/dc converter for reducing conduction losses," *IEEE Trans. Power Electron.*, vol.14, no.2, pp.258–264, Mar. 1999.

[16] J. G. Cho, C.Y. Jeong, and F.C. Lee, "Zero-voltage and zero-current-switching full-bridge PWM converter using secondary active clamp," *IEEE Trans. Power Electron.*, vol.13, no.4, pp.601–607, Jul. 1998.

[17] Francisco Canales, Peter Barbosa, and Fred C. Lee, "A zero-voltage and zero-current switching three-level dc/dc converter," *IEEE Trans. Power Electron.,* vol.17, no.6, pp.898–904, Nov. 2002.

[18] Yo.-S. Shin, S.-S. Hong, D.-J. Kim, D. -S. Oh, and S.-K. Han, "A new mode changeable full bridge dc/dc converter for wide input voltage range," in *Proc. 8th International Conference on Power Electronics - ECCE Asia* (ICPE), May 2011, pp.2328–2335.

[19] J.G. Cho, J.A. Sabate, G. Hua, Member, and F.C. Lee, "Zero-voltage and zero-current-switching full bridge PWM converter for high-power applications," *IEEE Trans. Power Electron.*, vol.11, no.4, pp.622–628, Jul. 1996.

[20] X. Ruan and Y. Yan, "Novel zero-voltage and zero-current-switching PWM full-bridge converter using two diodes in series with the lagging leg", *IEEE Trans. Ind. Electron.*, vol.48, no.4, pp.777–785, Aug. 2001.

[21] S. Moiseev, K. Soshin, and M. Nakaoka, "Tapped-inductor filter assisted soft switching PWM dc-dc power converter," *IEEE Trans. Aerospace and Electronic System*, vol.41, no.1, pp.174–179, Jan. 2005.

[22] K. M. Cho, Y. D. Kim, I. H. Cho, and G. W. Moon, "Transformer integrated with additional resonant inductor for phase-shift full-bridge converter with primary clamping diodes," *IEEE Trans. Power Electron.* vol.27, no.5, pp.2405–2414, May 2012.

[23] J. Zhang, F. Zhang, X. Xie, and D. Jiao, and Z. Qian, "A novel ZVS dc/dc converter for high power applications", *IEEE Trans. Power Electron.*, vol.19, no.2, pp.420–429, Mar. 2004.

[24] T. Mishima and M. Nakaoka, "Practical evaluations of a ZVS-PWM dc-dc converter with secondary-side phase-shifting active rectifier", *IEEE Trans. Power Electron.*, vol.26, no.12, pp. 3896–3907, Dec. 2011.

[25] S. Hamada and M. Nakaoka, "Analysis and design of a saturable reactor assisted soft-switching full-bridge dc-dc converter," in *IEEE Trans. Power Electron.*, vol.9, pp.309–317, May 1994.

[26] T. Morimoto, S. Shirakawa, O. Koudriavtsev and M. Nakaoka, "Zero-voltage and zero-current hybrid soft-switching phase-shifted PWM dc-dc converter for high power applications", in *Proc. IEEE Applied Power Electronics Conference and Expositions* (IEEE-APEC), 2000, vol.1, pp.104–110.

[27] T. Mishima, K. Akamatsu and M. Nakaoka, "A zero voltage and zero current soft switching PWM dc-dc converter with secondary-side phase-shifting active rectifier", in *Proc. 2012 IEEE Energy Conversion Congress and Exposition* (ECCE-USA), Sept. 2012, pp.2544–2551.

[28] T. Mishima, K. Akamatsu and M. Nakaoka, "Analysis, design and evaluations of a soft switching PWM dc-dc converter with phase shift-controlled ZCS active hybrid rectifier", in *Proc. Annual Conference of the IEEE Industrial Electronics Society* (IEEE-IECON), pp.243–248, Oct. 2012.

[29] K. Akamatsu, T. Mishima, and M. Nakaoka, "A zero voltage and zero current soft-switching PWM dc-dc converter with synchronous phase shifting hybrid rectifier," in *Proc. 2013 IEEE Applied Power Electronics Conference and Expositions* (IEEE-APEC), Mar. 2013, pp.1–6.

**Tomokazu Mishima** (S'00–M'04) received the B.S., M.S., and Ph.D. degree all in electrical engineering from The University of Tokushima, Japan in 1999, 2001, and 2004 respectively. Since 2010, he has been with Kobe University, Hyogo, Japan as an associate professor, and engages in the researches and developments of power electronics circuits and systems. His research interests include soft-switching dc–dc converters, resonant converters, and high frequency inverters for industrial, automotive, renewable and sustainable energy applications.

Dr. Mishima received the Best Paper Award in the Eighth IEEE International Conference on Power Electronics and Drive Systems (IEEE-PEDS 2009). He serves as an associate editor for the special issue on Transportation Electrification and Vehicle Systems 2013 in IEEE Transaction on Power Electronics Society.

Dr. Mishima is a member of IEEJ (The Institute of Electrical Engineering of Japan), IEICE (The Institute of Electronics, Information and Communication Engineers), IEIEJ (The Institute of Electrical Installation of Japan), JIPE (The Japan Institute of Power Electronics), and JIME (The Japan Institute of Marine Engineering).

**Kouhei Akamatsu** (S'13) received the M.S. degree in the marine engineering from Kobe University, Japan in 2013, where he worked on the research of soft-switching dc-dc power converters suitable for automotive and renewable energy applications. Since 2013, he has been with the Toyota Industries Corporation, Aichi, Japan, and engages in the research and development of power electronics circuit and systems.

Mr. Akamatsu is the recipient of 2013 IEEE Applied Power Electronics Conference and Exposition (APEC) Student Competition Attendance Grant Award.

**Mutsuo Nakaoka** (M'83) received the Ph.D. degree in electrical engineering from Osaka University, Osaka, Japan, in 1981. From 1995 to 2004, he was a professor with the Graduate School of Science and Engineering, Yamaguchi University, Yamaguchi, Japan, and is currently a professor emeritus. Since 2004, he has been a visiting professor with Kyungnam University, Masan, Republic of Korea, and The University of Malaya, Kuala Lumpur, Malaysia since 2010. His research interests include applications and developments of power electronics circuits and systems for industrial electronics and home appliances. From 2001 to 2006, he served as Chairman of the IEEE-IES Japan Chapter.

Prof. Nakaoka received many distinguished paper awards on power electronics such as the 2001 Premium Prize Paper Award from IEE-UK, the 2001/2003 IEEE-IECON Best Paper Award, the Third Paper Award in 2000 IEEE-PEDS, the 2003 IEEE-IAS James Melcher Prize Paper Award, and the Best Paper Award of IAS-IATC ' 06, IEEE-PEDS 2009 Best Paper Awards, and IEEE-ISIE 2009 Best Paper Award.

Prof. Nakaoka is a member of IEEJ, IEICE, IEIEJ, and JIPE.